Journal of ELECTRONIC MATERIALS, Vol. 49, No. 8, 2020
https://doi.org/10.1007/s11664-020-08241-4

Improved Thermoelectric Performance in TiO_2 Incorporated Polyaniline: A Polymer-Based Hybrid Material for Thermoelectric Generators

AJIT DEBNATH,[1] KRISHNA DEB,[1] KAMANASHIS SARKAR,[1] and BISWAJIT SAHA [1,2]

1.—Department of Physics, National Institute of Technology Agartala, Jirania, West Tripura 799046, India. 2.—e-mail: biswajit.physics@gmail.com

Enhanced thermoelectric performances have been achieved in hybrid nanocomposites of TiO_2 incorporated into electrically conductive polyaniline (PANI) through a chemical polymerization process, for next-generation energy sources. Different weight percentages of TiO_2 were used in hybrid nanocomposites and their charge transport properties were studied to understand the consequence of TiO_2 incorporation in the PANI matrix. Aniline was used as reactant, and ammonium peroxydisulfate as polymerizing agent during synthesis process. The hybrid composites of TiO_2 incorporated PANI were studied by using X-ray diffraction pattern, Fourier transform-infrared spectra and scanning electron microscopic images. The thermoelectric characteristics of this PANI-based composite were much improved as compared to pure PANI. The ordered chain structures of PANI, and the decrease of carrier hopping barrier with incorporation of TiO_2 nanoparticles in the PANI chain matrix improved the charge carrier conduction and lead towards enhanced thermoelectric properties of these materials. The maximum Seebeck coefficient (S) as recorded 1.767 mV/°C, was fivefold larger as compared with pure PANI. The analysis of results reveal that these hybrid composites are potential candidates for next-generation thermoelectric generators with their light weight, environmentally friendly nature and cost-effectiveness for energy harvesting applications.

(Received January 6, 2020; accepted May 27, 2020; published online June 8, 2020)

Graphic Abstract

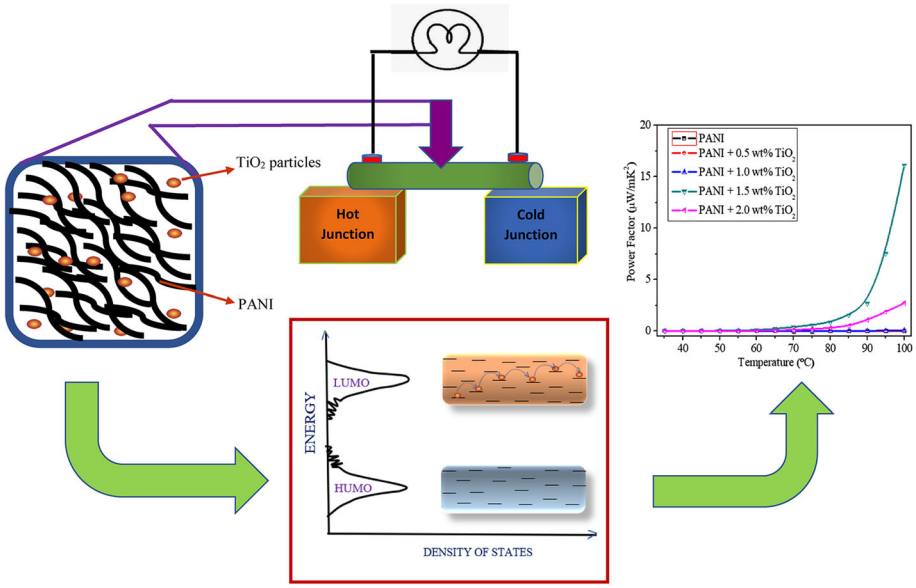

Key words: Charge transport, thermoelectric effect, Seebeck coefficient

INTRODUCTION

Thermoelectric generators are one of the most useful candidates in green energy conversion systems. Consequently, thermoelectric materials have attracted a greater recent attention in direct conversion of thermal energy into electrical energy without producing any waste or noise.[1–5] Research on development of thermoelectric generators with high performance is based on two important facts, firstly developing an appropriate system of materials, and secondly realizing molecular level engineering in achieving better thermoelectric figure of merit.[6,7] Compared with inorganic thermoelectric materials, conducting polymers, such as polyaniline (PANI),[8–11] poly(3,4-ethylenedioxythiophene) (PEDOT),[12–14] polypyrrole (PPy),[15,16] polyacetylene[17] and polythiophene[18,19] have been studied by many researchers as high performing thermoelectric materials, due to their unique features such as low density, cost effectiveness, and their ease of synthesis technique as well as scope of sample processing into different adaptable forms. The interchain and intrachain carrier hopping controls the carrier transport significantly in the conducting polymers following the variable range hopping (VRH) model.[20] In the conducting polymers family, PANI is one of the most promising, having an extensive area of applications such as semiconductors, sensors and biosensors, capacitors and supercapacitors, and polymer-based batteries,[21–28] because of its added advantages of tuneable electrical properties, low thermal conduction property, good environmental stability and nontoxicity.[29–31]

To improve thermoelectric properties of the nanocomposites, many attempts have been made by researchers such as by carrier energy filtering,[32] forming resonant states at the Fermi level[33,34] and carrier pocket engineering.[35,36] In order to enhance thermoelectric efficiency, the electronic and phononic properties of thermoelectric materials have been tailored by nanostructural engineering.[5,37–40] Still there are issues of developing thermoelectric materials with cost effectiveness, large-scale producibility and high thermoelectric functionality. With this in mind, we have attempted to improve the power factor ($S^2\sigma$) of the π conjugated PANI induced by the strong interaction amongst PANI and TiO_2 nanoparticles.

In this work, we have sought to lower the hopping barrier height for the carriers to improve the thermoelectric power factor by incorporating TiO_2 in the PANI matrix. For this, TiO_2 nanoparticles and PANI have been prepared through sol–gel and chemical polymerization techniques, respectively, and their hybrid PANI/TiO_2 composites have been synthesized by a chemical polymerization[41] at comparatively lower temperature using different weight percentages of TiO_2. The prepared PANI/TiO_2 composites have been studied extensively to explore the

effect of TiO_2 incorporation in PANI on their physical properties. Analysis of the results of electrical transport and thermoelectric measurements reveals a notable improvement in thermoelectric properties, and this has been realized from the effective decrease of hopping barrier height in the well-arranged chain structure of polymer. A strong interaction among conjugated PANI and TiO_2 nanoparticles plays the key role in achieving these improvements in the PANI/TiO_2 composites. In the context of other previous reports, the significance of this work lies on the outstanding enhancement of Seebeck coefficient.[42–45] The maximum Seebeck coefficient was obtained 1.767 mV/°C with a temperature difference of only 100°C. Nontoxicity, simplicity of synthesis and disposability of such electronic garbage extends the broader advantages this work over other previous reports on inorganic based thermoelectric materials.

EXPERIMENTAL PROCEDURE

Materials

In this work the chemicals used were aniline (99.5%) monomer, titanium isopropoxide ($C_{12}H_{28}O_4Ti$), ammonium peroxydisulfate (APS), hydrochloric acid (HCl) and methanol (CH_3OH, 99.9% ethanol absolute, Merck). Double distillation process was used to purify the aniline before polymerization, while deionized water was used for washing and preparing aqueous solution.

Synthesis of TiO_2 Nanoparticles

To synthesize nanocrystalline TiO_2, the sol-gel process has been used with titanium isopropoxide as a source of Ti.[46] In a typical synthesis process, 6.0 mL of titanium isopropoxide was dispersed into methanol of volume 70.0 mL. It was then stirred for 5 h vigorously at temperature 80°C by a magnetic stirrer. A white powder was formed, which was separated through filtration and sintered at 500°C for 2 h to obtain TiO_2 powder.

Synthesis of Conductive PANI

Conductive PANI powder was synthesized by chemical polymerization. First, a dilute acid solution (0.5 M) of HCl was taken in a beaker, and then 0.1 M double-distilled aniline monomer was added into the beaker at a volume ratio of 5:1 and stirred vigorously maintaining its temperature below 5°C in an ice bath. Ammonium persulfate (APS) was prepared in another beaker of strength 0.1 M. Then the APS solution was added drop wise into the acidic aniline solution gently. APS acted as polymerizing agent (initiator) for aniline. A deep precipitate was obtained under continuous stirring, and it was collected by filtration. The separated precipitates have been washed several times using distilled water followed by wash in methanol to eliminate the oligomeric impurities. Then PANI powder was obtained after drying at temperature of 60–70°C for 8 h.

Preparation of PANI/TiO_2 Composites

Hybrid TiO_2 incorporated PANI composites have been obtained by an in situ chemical reaction of polymerization at a temperature below 5°C with different weight percentages of TiO_2.[47] In a typical synthesis, 0.5 M HCl and 0.1 M aniline monomer were stirred with double-distilled water, and TiO_2 nanopowder was dispersed in the solution. Then, with constant stirring, the initiator (APS solution) was mixed dropwise into the solution. The colour of the solution changed to light blue,[48] during the reaction indicating the formation of PANI. To ensure complete polymerization, the stirring was continued for next 5 h. Through the process of filtration and several wash in methanol, a dark green colored nanocomposite of PANI/TiO_2 was finally separated. The obtained product was dried in an oven at 60°C for 12 h, as unreacted aniline if any, will be vaporized at that temperature. These processes of preparation of PANI/TiO_2 nanocomposite were repeated with 1.0 wt.%, 1.5 wt.% and 2.0 wt.% of TiO_2. Fine powders of nanocomposites were obtained through grinding those with a mortar and pestle.

Characterizations

The prepared hybrid nanocomposites of TiO_2 incorporated PANI were studied with different characterization techniques to study the structural, compositional, optical, electrical and thermoelectric properties. Structural characterization of the prepared samples was performed at room temperature using Bruker D-8 Advance X-ray powder

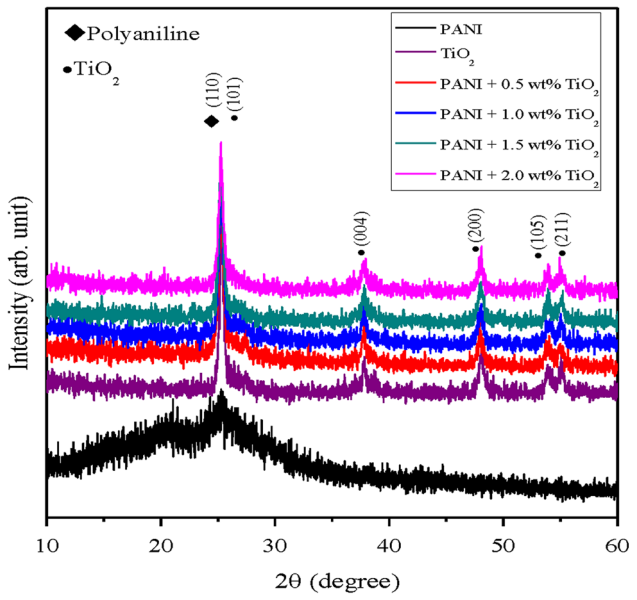

Fig. 1. XRD patterns of pure PANI, TiO_2 and the different samples of PANI/TiO_2 nanocomposites.

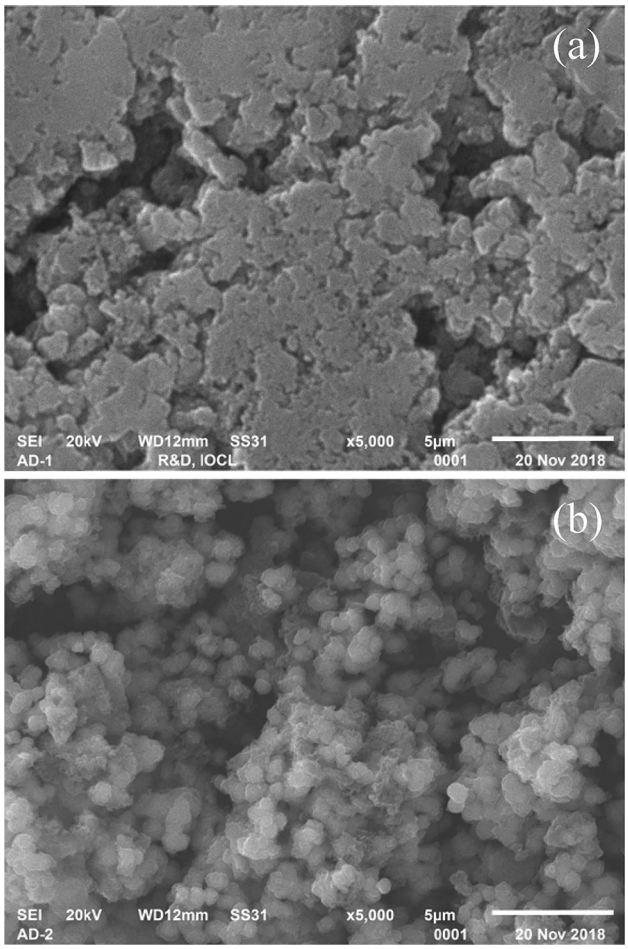

Fig. 2. SEM images of (a) pure PANI (b) PANI/TiO_2 composites with 1.5 wt.% TiO_2.

diffractometer (XRD) with Cu-Kα (λ = 1.54 Å) radiation. The scanning electron microscopy (SEM) measurement was done to observe the surface topography of the samples. To analyse chemical bonding configurations of PANI and PANI/TiO_2 composites, Fourier transform infrared (FTIR) spectroscopy was studied using an FTIR system (Perkin-Elmer FTIR 1700 Spectrometer). The optical properties were analysed from UV–Vis–NIR absorption spectra taken by a Shimadzu 3600 plus spectrometer. An Agilent (U3606B) source meter unit was used for electrical and thermoelectric measurements.

RESULTS AND DISCUSSION

Structural and Morphological Characterization

Crystal structure analyses of the hybrid composites are of high significance in charge transport properties of such systems, and was studied from the XRD patterns of the composites as shown in Fig. 1. Occurrence of different prominent diffraction peaks for the PANI/TiO_2 composites indicates their crystalline and orderly arrangement in the system.

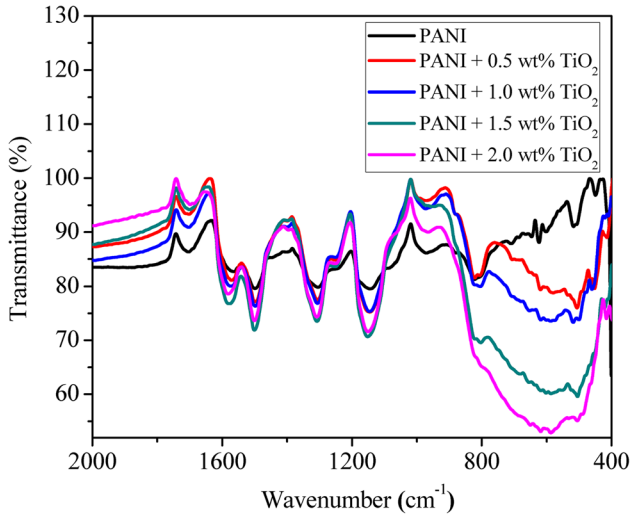

Fig. 3. FTIR spectra PANI and TiO_2 incorporated PANI composites.

The peak occurred at $2\theta = 25.10°$ in the XRD pattern of pure PANI corresponds to miller plane (110) of PANI.[49] For PANI/TiO_2 nanocomposites the X-ray diffraction peaks occurred at $2\theta = 25.20°$, 37.90°, 48.10°, 54.10° and 55° corresponding to (101), (004), (200), (105) and (211) reflection planes of TiO_2 respectively.[50] Incorporation of crystalline TiO_2 with PANI provides higher mobility to the charge carriers; however, TiO_2 may act as scattering centres for phonon assisted thermal conduction and thus provide better thermoelectric performances. The morphology of the prepared PANI/TiO_2 composites has been observed from scanning electron microscopic (SEM) images. Figure 2 depicts a typical SEM image of PANI and that of a PANI/TiO_2 composite. The nanostructure of PANI in the hybrid nanocomposite is greatly influenced by the addition of TiO_2. It is clearly visible from the images that the composites have smaller grain size as compared with that of pure PANI.

Fourier Transform Infrared Spectral Analysis

In order to observe the chemical bonding configurations of the prepared PANI/TiO_2 nanocomposites, room temperature FTIR spectra in the frequency range of 400–4000 cm^{-1} were studied, which is shown in Fig. 3. The occurrence of partially oxidized emeraldine form of PANI along with TiO_2 in the nanocomposite has been confirmed from presences of various characteristic peaks of PANI and TiO_2 in the spectra. Incorporation of TiO_2 with PANI does not alter the chemical bonding configuration and oxidation state of PANI in the composite. In the FTIR spectra the band occurred at 1705 cm^{-1} is caused by the C=O stretching vibration of COOH.[51] The peaks in the FTIR spectra at 1496 cm^{-1} and 1562 cm^{-1} have been observed due to benzenoid and quinonoid ring stretching vibration respectively, while that at 823 cm^{-1} is because of out-of-plane C–H bending vibration.[52] The FTIR

absorbance peaks appeared due to the C–N stretching mode are observed at 1306 cm^{-1} and 1239 cm^{-1}.[48] The peak occurred at 1139 cm^{-1} corresponds to the vibration mode of the $-NH^{+}=$ structure, and it is formed during protonation.[53] The peak obtained at 969 cm^{-1} represents the C–H bands of benzenoid group of PANI.[54] In the spectrum of PANI/TiO_2 nanocomposites, the Ti-O-Ti bending mode gives raise to the wide peak occurred at around 500–700 cm^{-1}.[55]

Optical Properties

The optical properties of PANI/TiO_2 are of profound significance in analysing the formation of defect levels in band diagram. Figure 4 shows the optical absorbance spectra of the PANI and TiO_2 incorporated PANI. The peak at 326 nm for pure PNAI in the UV–Vis absorption spectrum corresponds to the π–π^* electron orbital transition. Another peak corresponding to quinoid rings (n–π^*) exciton absorption at around 600–620 nm was obtained.[56,57] In PANI/TiO_2 nanocomposites, a slight but gradually increasing blue shift with increasing TiO_2 incorporation in polymer matrix was observed for the peak at around 326 nm. Further the occurrence of partially oxidized emeraldine state of PANI in the PANI/TiO_2 nanocomposite has been designated by the characteristic features in the absorption spectrum. Thus, the PANI/TiO_2 composites also exhibit electrical conductivity similar to that of conductive state of PANI. An additional absorption peak has been observed at around 452 nm for the PANI/TiO_2 nanocomposite, which may be due to the existence of titanium dioxide nanoparticles in the nanocomposite. This defect state may be produced due to large number of localized states along the polymer chain backbone.

The optical absorption spectra have been studied to obtain the optical band gap and its variation due to TiO_2 nanoparticles incorporation in PANI. Using the fundamental relation among the incident photon energy ($h\nu$) and the optical absorption coefficient (α), the optical band gap has been obtained using the relation

$$\alpha h\nu = A\left(h\nu - E_g\right)^n \quad (1)$$

where α, ν, E_g and A stands for absorption coefficient, frequency of photon, band gap energy, and a constant, respectively. For different types of transitions, the exponent n has different values. From the linear extrapolation of $(\alpha h\nu)^2$ versus $(h\nu)$ plot (Fig. 5) the optical energy band gaps have been determined. The optical band gap of PANI is 2.94 eV, and that of PANI/TiO_2 with 0.5%, 1.0%, 1.5% and 2.0% wt.% of TiO_2 have values of 2.63 eV, 2.58 eV, 2.45 eV and 2.56 eV, respectively. This shows decrease of optical band gap by incorporation of TiO_2 in PANI; however, with excessive TiO_2 content in PANI the band gap again starts to increase.

The initial decrease in optical band gap indicates the formation of in gap defect states due to TiO_2 incorporation. The degree of disorder and the presence of defects, according to Mott and Devis control the width of the mobility edge. Localized states are produced by defects in the forbidden gap.[58] However, with excess content of TiO_2, the optical band gap increases as it breaks into smaller crystallites.

Electrical and Thermoelectric Properties

Thermoelectric performance of a material is dependent on a number of parameters such as electrical conductivity, Seebeck coefficient, and thermal conductivity. The prime objective of this work was to enhance the thermoelectric performance of PANI with incorporation of TiO_2. This is based on the charge carrier dynamics of such organic inorganic hybrid system. It has been observed that the electrical conductivity of PANI

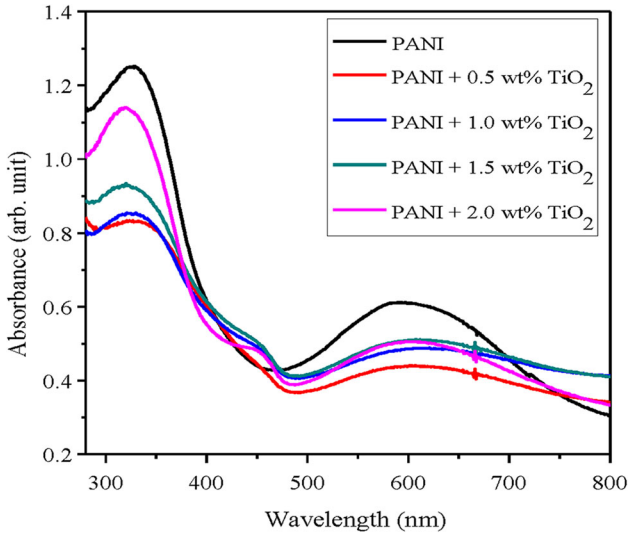

Fig. 4. Optical absorbance plot of PANI and PANI/TiO_2 composites recorded at room temperature.

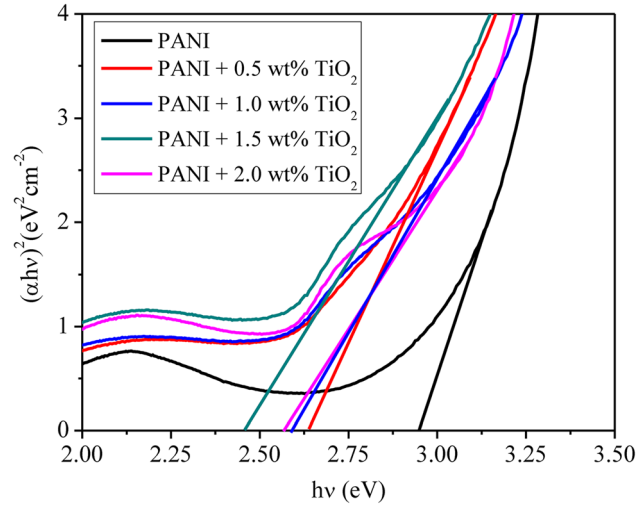

Fig. 5. $(\alpha h\nu)^2$ versus $(h\nu)$ plot of PANI and PANI/TiO_2 composites.

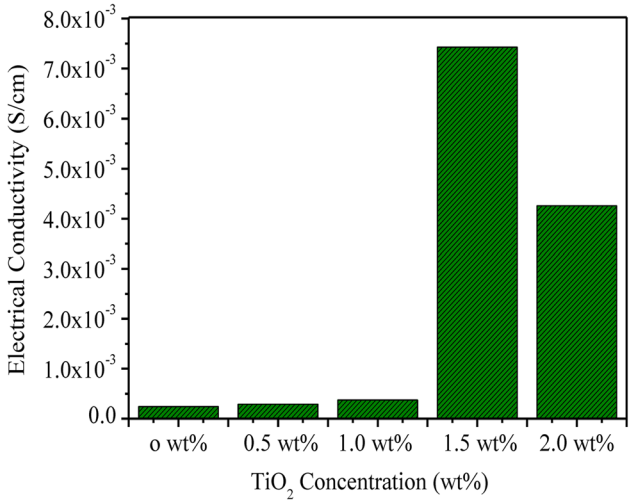

Fig. 6. Room temperature electrical conductivity for pure PANI and PANI/TiO_2 composites.

has been improved significantly with incorporation TiO_2. Figure 6 represents the variation of room temperature electrical conductivity with different amount of TiO_2 incorporation.

With increasing weight percentage of TiO_2 from 0.5% to 1.5%, the electrical conductivity of the PANI/TiO_2 composites remarkably enhanced from 0.000805 S/cm to 0.052 S/cm. The maximum electrical conductivity is 84 times higher than that of PANI. This higher conductivity (0.052 S/cm) is due to the formation of more conductive pathways in the composite. TiO_2 in polymeric system brings two major improvements: firstly, TiO_2 in interaction with PANI creates more planar arrangement of polymer chains providing better interchain carrier transport; secondly, TiO_2 reduces the carrier hopping barrier potential. Both effects result in significant enhancements of electrical conductivity of the hybrid system of TiO_2 incorporated PANI.

However, the electrical conductivity of the PANI/TiO_2 composite was slightly decreased, with TiO_2 content more than 1.5 wt.%. This may be because carriers are unable to hop between favourable localized sites due to the hindering of conducting paths formed by insulating barriers in the PANI/TiO_2 composites with high TiO_2 content.

In order to investigate the charge carrier dynamics in the hybrid system of PANI/TiO_2 nanocomposites, the temperature dependence of their electrical conductivity become highly significant. The variation of electrical conductivity of PANI/TiO_2 nanocomposites with temperature has been depicted in Fig. 7. The electrical conductivity of the composites increases nonlinearly with increasing temperature, signifying a characteristic behaviour of non-metallic electrical conduction. The nonlinearity in the curve indeed shows that variable-range hopping is dominating the electrical conduction mechanism.[18]

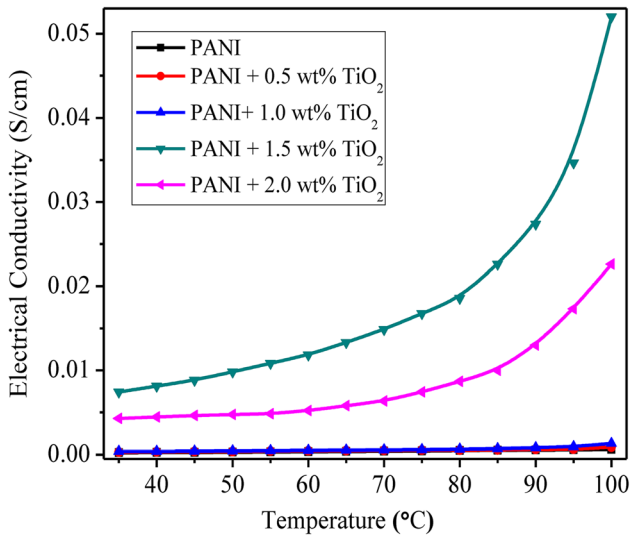

Fig. 7. Temperature dependence of electrical conductivity of PANI and PANI/TiO_2 composites.

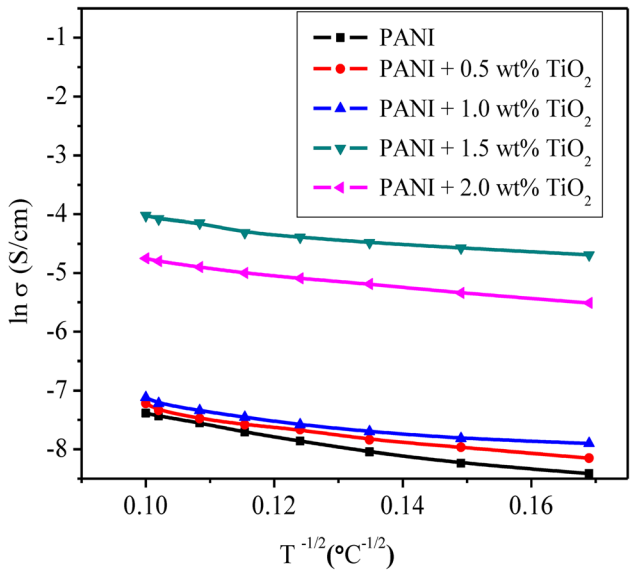

Fig. 8. ln σ versus $T^{-1/2}$ plot of pure PANI and PANI/TiO_2 composites.

The characteristic Mott temperature (T_0) has been calculated using the relation as follows

$$\sigma(T) = \sigma_0 \exp\left[\frac{T_0}{T}\right]^{\frac{1}{2}} \quad (2)$$

where T_0 is the characteristic Mott temperature, σ_0 is a constant. T_0 is dependent on hopping barrier of carriers. It is considered that the conduction mechanism of PANI follows the quasi-one-dimensional variable range hopping (1D-VRH) model.[20]

Figure 8 shows that the ln σ versus $T^{-1/2}$ plot appears as a straight line indicating the hopping conduction. Further, the values of T_0 have been

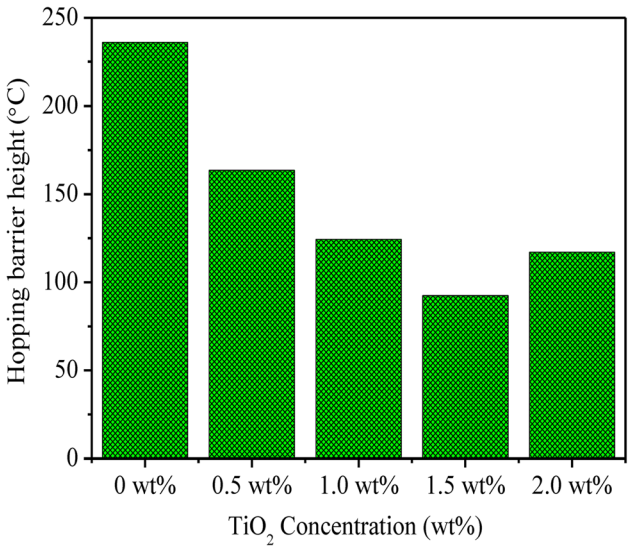

Fig. 9. Calculated values of carrier hopping barrier (in terms of T_0) of pure PANI and PANI/TiO_2 hybrid composites.

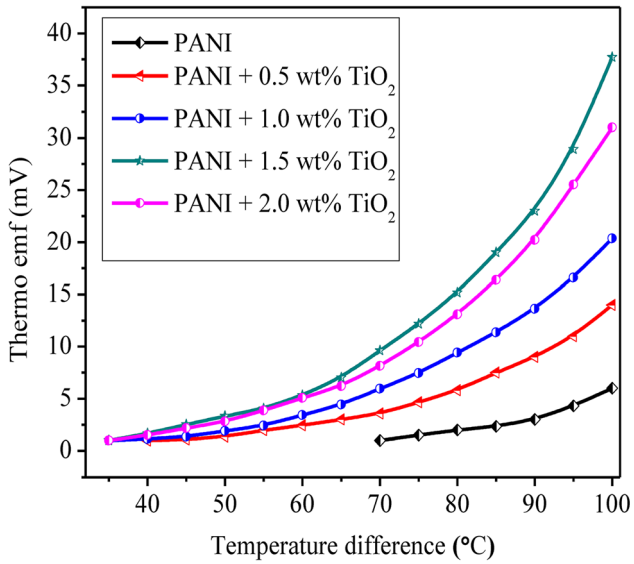

Fig. 10. Variation of thermo emf with temperature difference.

calculated using the gradient of the straight lines. T_0 are obtained to be 236.0°C for pure PANI, while 163.5°C, 124.3°C, 92.5°C and 117.0°C for PANI/TiO_2 nanocomposite with 0.5%, 1.0%, 1.5% and 2.0% of TiO_2 content. The values of T_0 indicate that the hopping barrier is reduced in the PANI/TiO_2 nanocomposites as compared to that of pure PANI. The hopping rate amongst the neighbouring localized states thus increases and contributes in enhanced electrical conductivity in PANI/TiO_2 composites.[59] The changes in hopping barrier has been depicted in Fig. 9.

These noteworthy enhancements in electrical properties are the motivation for the investigation of the thermoelectric properties of the hybrid composites. The thermo emf of pure PANI and that of TiO_2 incorporated PANI have been measured and shown in Fig. 10. The temperature of the cold end was kept fixed at 0°C and the temperature of the hot end varied. The results and plots are presented with respect to the temperature of the hot end. One can observe a systematic increase the thermo emf of the composites up to a certain level of TiO_2 incorporation. Further, a noteworthy 38.0 mV of thermo emf was recorded at a temperature difference of only 100°C. However, with excessive TiO_2 incorporation, the thermo emf decreased. This is in agreement with the behaviour of electrical conductivity and may be due to the same reason of decrease of electrical conductivity.

The variation of Seebeck coefficient for the pure PANI and its composite samples with varying TiO_2 concentration temperature is shown in Fig. 11. The positive Seebeck coefficient confirms that holes are the majority charge carriers. With increasing content of TiO_2 nanoparticles in the composites, the Seebeck coefficient increased up to a TiO_2 content of 1.5%, and the Seebeck coefficient slightly decreased

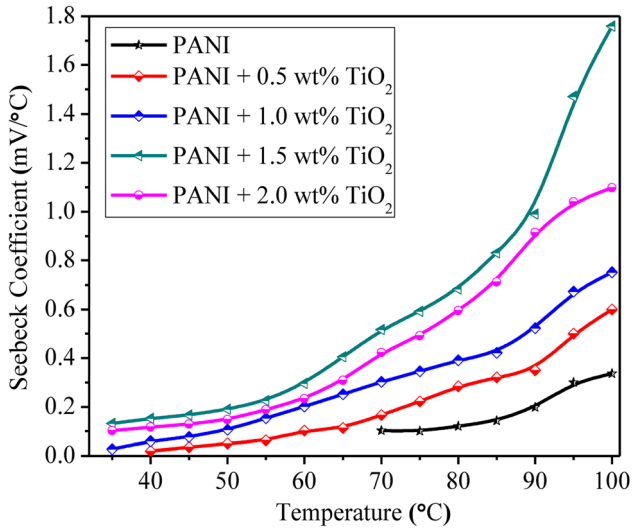

Fig. 11. Variation of Seebeck coefficient (S) with temperature.

with a further increase in TiO_2. The thermoelectric performance, and hence Seebeck coefficients, are essentially dependent on the charge transport process in the polymer system. The degree of order of polymer chain considerably influences the charge transport in the polymeric system. The barriers of intrachain and interchain hopping are effectively reduced by highly oriented polymer chains and facilitate easy movement of carriers. When TiO_2 was introduced into the PANI system, both TiO_2 and PANI appeared in crystalline form with higher ordering. Consequently, PANI grew with a more ordered molecular chain packing providing higher conductivity. Further, the formation of interfaces between PANI and TiO_2 may contribute to phonon scattering and thus increases the Seebeck

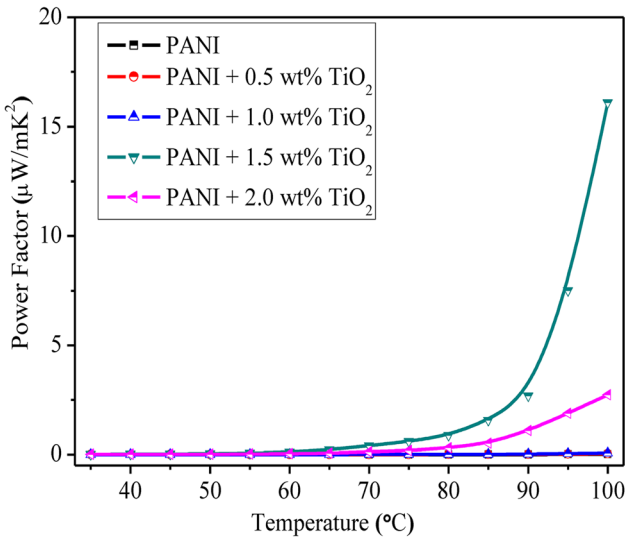

Fig. 12. Power factor versus temperature plot of PANI and PANI/TiO_2 composites.

coefficient. In addition, it is observed for each sample that with the increasing temperature, the Seebeck coefficient increases. The Seebeck coefficient has been recorded to be as much as 1.767 mV/°C, at a temperature difference of only 100°C. This indicates that these PANI/TiO_2 nanocomposites will be suitable for designing thermoelectric generator operating with low temperature difference, nevertheless with significant electric power output.

The power factor (PF) of a thermoelectric material is a useful indicator to its thermoelectric performance. The higher values of PF of a thermoelectric material indicate its better applicability in thermoelectric generators. The PF of thermoelectric material is denoted by PF = $S^2\sigma$. Thus, to achieve higher value of PF for a thermoelectric material, it requires higher values of both σ and S. The variation of power factor with temperature of the hot end has been depicted in Fig. 12.

The maximum power factor was recorded for the PANI/TiO_2 nanocomposite with 1.5% of TiO_2, and it was observed to be increasing with increase in temperature difference. In this work a thermoelectric power factor as much as 16.17 $\mu W/mK^2$ has been recorded for PANI/TiO_2 nanocomposite at a temperature difference of only 100°C. This value is remarkably high as compared with many of such recently reported thermoelectric materials.[60–66]

CONCLUSION

In summary, hybrid PANI/TiO_2 composites were successfully obtained through a chemical polymerization process. The XRD results revealed that the TiO_2 incorporated PANI chain matrix in the hybrid composite have better molecular arrangement than that of pure PANI. Easy carrier propagation in the ordered molecular arrangement along with reduced interchain and intrachain hopping barriers of the polymer chain matrix have been the key achievement of this work. Consequently, TiO_2 incorporation leads to enhanced electrical conductivity with simultaneous improvement of the Seebeck coefficient of the hybrid PANI/TiO_2 nanocomposites. It exhibits the best performance at 1.5 wt.% of TiO_2. The maximum electrical conductivity and Seebeck coefficient of the TiO_2 incorporated PANI hybrid composites were found to be 0.052 S/cm and 1.767 mV/°C, which are remarkably higher than those of pure PANI. Consequently, an exceptionally high power factor with a maximum recorded value of 16.17 $\mu W/mK^2$, has been realized. This enhanced power factor is caused by the lowering of hopping barrier potential achieved through TiO_2 incorporation in PANI. Thus, PANI incorporated with TiO_2 has application in thermoelectric generators with such enhanced performance.

ACKNOWLEDGMENTS

The authors acknowledge the CRF of NIT Agartala for extending XRD measurement facility and DST-FIST program (SR/FST/PSI-196/2014) for UV–Vis–NIR measurement facility. The authors also acknowledge the financial assistance provided through the Minor (Seed) Research Grants scheme under TEQIP III of NIT Agartala.

REFERENCES

1. T.C. Harman, P.J. Taylor, M.P. Walsh, and B.E. LaForge, *Science* 297, 2229 (2002).
2. S. Shin, S. Bang, J. Choi, H.J. Son, H. Yoon, H. Yun, J.H. Choi, and D. Wee, *Int. J. Energy Res.* 39, 851 (2015).
3. H. Hazama, Y. Masuoka, A. Suzumura, M. Matsubara, S. Tajima, and R. Asahi, *Appl. Energy* 226, 381 (2018).
4. L. Li, S. Xu, and G. Li, *Energy Technol.* 3, 825 (2015).
5. C. Lundgaard and O. Sigmund, *Appl. Energy* 236, 950 (2019).
6. K. Ahmad, C. Wan, and M.A. Al-Eshaikh, *J. Electron. Mater.* 46, 1348 (2017).
7. M. Culebras, M.M. de Lima Jr, C. Gómez, and A. Cantarero, *J. Appl. Polym. Sci.* 134, 43927 (2017).
8. X.Y. Wang, C.Y. Liu, L. Miao, J. Gao, and Y. Chen, *J. Electron. Mater.* 45, 1813 (2016).
9. H. Anno, M. Hokazono, F. Akagi, M. Hojo, and N. Toshima, *J. Electron. Mater.* 42, 1346 (2013).
10. B. Zheng, Y. Liu, B. Zhan, Y. Lin, J. Lan, and X. Yang, *J. Electron. Mater.* 43, 3695 (2014).
11. Y. Zhao, G.S. Tang, Z.Z. Yu, and J.S. Qi, *Carbon* 50, 3064 (2012).
12. S. Hata, K. Taguchi, K. Oshima, Y. Du, Y. Shiraishi, and N. Toshima, *ChemistrySelect* 4, 6800 (2019).
13. S. Maity, N. Sepay, C. Kulsi, A. Kool, S. Das, D. Banerjee, and K. Chatterjee, *ChemistrySelect* 3, 8992 (2018).
14. A.K. Kyaw, T.A. Yemata, X. Wang, S.L. Lim, W.S. Chin, K. Hippalgaonkar, and J. Xu, *Macromol. Mater. Eng.* 303, 1700429 (2018).
15. M. Bharti, P. Jha, A. Singh, A.K. Chauhan, S. Mishra, M. Yamazoe, A.K. Debnath, K. Marumoto, K.P. Muthe, and D.K. Aswal, *Energy* 176, 853 (2019).
16. C. Li, H. Ma, and Z. Tian, *Appl. Therm. Eng.* 111, 1441 (2017).
17. Y. Du, S.Z. Shen, W.D. Yang, K.F. Cai, and P.S. Casey, *Synth. Met.* 162, 375 (2012).
18. L. Wang, X. Jia, D. Wang, G. Zhu, and J. Li, *Synth. Met.* 181, 79 (2013).
19. Z. Golsanamlou, M.B. Tagani, and H.R. Soleimani, *Theory Simul.* 23, 311 (2014).

20. Q. Yao, L. Chen, W. Zhang, S. Liufu, and X. Chen, *ACS Nano* 4, 2445 (2014).
21. M.A. Soto-Oviedo, O.A. Araujo, R. Faez, M.C. Rezende, and M.A. De Paoli, *Synth. Met.* 156, 1249 (2006).
22. K. Deb, A. Debnath, A. Bera, K. Sarkar, A. Debnath, and B. Saha, *Surf. Interfaces* 16, 141 (2019).
23. J. Dominic, T. David, A. Vanaja, G. Muralidharan, N. Maheswari, and K.K. Satheesh Kumar, *Appl. Surf. Sci.* 460, 40 (2018).
24. K. Deb, A. Bera, and B. Saha, *RSC Adv.* 6, 94795 (2016).
25. Z. Guo, N. Liao, M. Zhang, and W. Xue, *Appl. Surf. Sci.* 453, 336 (2018).
26. K. Deb, A. Bera, K.L. Bhowmik, and B. Saha, *Polym. Eng. Sci.* 58, 2249 (2018).
27. H. Zheng, N.M. Ncube, K. Raju, N. Mphahlele, and M. Mathe, *Springer Plus* 5, 630 (2016).
28. E. Zanzola, C.R. Dennison, A. Battistel, P. Peljo, H. Vrubel, V. Amstutz, and H.H. Girault, *Electrochim. Acta* 235, 664 (2017).
29. M.S. Cho, S.Y. Park, J.Y. Hwang, and H.J. Choi, *Mater. Sci. Eng. C* 24, 15 (2004).
30. S.M. Reda and S.M. Al-Ghannam, *Adv. Mater. Phys. Chem.* 2, 75 (2012).
31. X.L. Wei, Y.Z. Wang, S.M. Long, C. Bobeczko, and A.J. Epstein, *J. Am. Chem. Soc.* 118, 2545 (1996).
32. Y.L. Ravich, B.A. Efimova, and V.I. Tamarchenko, *Exp. Phys. Status Solidi B* 43, 453 (1971).
33. L.D. Hicks and M.S. Dresselhaus, *Phys. Rev. B* 47, 16631 (1993).
34. J.P. Heremans, V. Jovovic, E.S. Toberer, A. Saramat, K. Kurosaki, A. Charoenphakdee, S. Yanmanaka, and G.J. Syndler, *Science* 321, 554 (2008).
35. T. Koga, S.B. Cronin, J.Y. Ying, M.S. Dresselhaus, J.L. Liu, and K.L. Wang, *Appl. Phys. Lett.* 77, 1490 (2000).
36. T. Koga, Ph.D. thesis (Harvard University, 2000).
37. B. Paul and P. Banerji, *Nanosci. Nanotechnol. Lett.* 1, 208 (2009).
38. B. Paul, A. Kumar V, and P. Banerji, *J. Appl. Phys.* 108, 064322 (2010).
39. P.K. Rawat, B. Paul, and P. Banerji, *Nanotechnology* 24, 215401 (2013).
40. P.K. Rawat, B. Paul, and P. Banerji, *ACS Appl. Mater. Interfaces* 6, 3995 (2014).
41. C. Bian, Y. Yu, and G. Xue, *J. Appl. Polym. Sci.* 104, 21 (2007).
42. F.P. Du, Q.Q. Li, P. Fu, Y.F. Zhang, and Y.G. Wu, *J. Mater. Sci. Mater. Electron.* 29, 8666 (2018).
43. C. Guo, F. Chu, P. Chen, J. Zhu, H. Wang, L. Wang, Y. Fan, and W. Jiang, *J. Mater. Sci.* 53, 6752 (2018).
44. H. Ju, D. Park, and J. Kim, *Polymer* 160, 24 (2019).
45. K. Sarkar, A. Debnath, K. Deb, A. Bera, and B. Saha, *Energy* 177, 203 (2019).
46. S.G. Pawar, S.L. Patil, M.A. Chougule, S.N. Achary, and V.B. Patil, *Int. J. Polym. Mater.* 60, 244 (2011).
47. S. Radhakrishnan, C.R. Siju, D. Mahanta, S. Patil, and G. Madras, *Electrochim. Acta* 54, 1249 (2009).
48. M.S. Lashkenari, S. Rezaei, J. Fallah, and H. Rostami, *Synth. Met.* 235, 71 (2018).
49. H. Xu, X. Chen, J. Zhang, J. Wang, B. Cao, and D. Cui, *Sens. Actuators B* 176, 166 (2013).
50. I. Gawri, R. Ridhi, K.P. Singh, and S.K. Tripathi, *Mater. Res. Express* 5, 025303 (2015).
51. M. Mitra, C. Kulsi, K. Kargupta, S. Ganguly, and D. Banerjee, *J. Appl. Polym. Sci.* 135, 46887 (2018).
52. S. Cui, J. Wang, and X. Wang, *RSC Adv.* 5, 58211 (2015).
53. K.L. Bhowmik, K. Deb, A. Bera, R.K. Nath, and B. Saha, *J. Phys. Chem. C* 120, 5855 (2016).
54. M. Campos, T.A.S. Miziara, F.H. Cristovan, and E.C. Pereira, *J. Appl. Polym. Sci.* 131, 40688 (2014).
55. N. Wang, J. Li, W. Lv, J. Feng, and W. Yan, *RSC Adv.* 5, 21132 (2015).
56. M. Mitra, C. Kulsi, K. Chatterjee, K. Kargupta, S. Ganguly, D. Banerjee, and S. Goswami, *RSC Adv.* 5, 31039 (2015).
57. K. Gupta, P.C. Jana, and A.K. Meikap, *J. Appl. Phys.* 109, 123713 (2011).
58. M.D.A. Khan, A. Akhtar, and S.A. Nabi, *New J. Chem.* 39, 3728 (2015).
59. S. Sarmah and A. Kumar, *Bull. Mater. Sci.* 36, 31 (2013).
60. F.P. Du, N.N. Cao, Y.F. Zhang, P. Fu, Y.G. Wu, Z.D. Lin, R. Shi, A. Amini, and C. Cheng, *Sci. Rep.* 8, 6441 (2018).
61. S.A. Gregory, A.K. Menon, S. Ye, D.S. Seferos, J.R. Reynolds, and S.K. Yee, *Adv. Energy Mater.* 8, 1802419 (2018).
62. Z. Zhang, G. Chen, H. Wang, and W. Zhai, *J. Mater. Chem. C* 3, 1649 (2015).
63. K. Chatterjee, M. Mitra, K. Kargupta, S. Ganguly, and D. Banerjee, *Nanotechnology* 24, 215703 (2013).
64. M. He, J. Ge, Z. Lin, X. Feng, X. Wang, H. Lu, Y. Yanga, and F. Qiu, *Energy Environ. Sci.* 5, 8351 (2012).
65. M. Bharti, A. Singh, S. Samanta, A.K. Debnath, K. Marumoto, D.K. Aswal, K.P. Muthe, and S.C. Gadkari, *Vacuum* 153, 238 (2018).
66. S. Xin, N. Yang, F. Gao, J. Zhao, L. Li, and C. Teng, *Mater. Chem. Phys.* 212, 440 (2018).